

Marco Ceccarelli
Eusebio Eduardo Hernández Martínez
Editors

Multibody Mechatronic Systems

Proceedings of the MUSME Conference
held in Huatulco, Mexico,
October 21–24, 2014

Mechanisms and Machine Science

Volume 25

Series editor

Marco Ceccarelli, Cassino, Italy

More information about this series at <http://www.springer.com/series/8779>

Marco Ceccarelli
Eusebio Eduardo Hernández Martínez
Editors

Multibody Mechatronic Systems

Proceedings of the MUSME Conference
held in Huatulco, Mexico,
October 21–24, 2014

Editors

Marco Ceccarelli
Laboratory of Robotics and Mechatronics
LARM
University of Cassino and South Latium
Cassino
Italy

Eusebio Eduardo Hernández Martínez
Section of Graduate Studies
National Polytechnic Institute
Mexico
Distrito Federal
Mexico

ISSN 2211-0984

ISBN 978-3-319-09857-9

DOI 10.1007/978-3-319-09858-6

ISSN 2211-0992 (electronic)

ISBN 978-3-319-09858-6 (eBook)

Library of Congress Control Number: 2014946398

Springer Cham Heidelberg New York Dordrecht London

© Springer International Publishing Switzerland 2015

This work is subject to copyright. All rights are reserved by the Publisher, whether the whole or part of the material is concerned, specifically the rights of translation, reprinting, reuse of illustrations, recitation, broadcasting, reproduction on microfilms or in any other physical way, and transmission or information storage and retrieval, electronic adaptation, computer software, or by similar or dissimilar methodology now known or hereafter developed. Exempted from this legal reservation are brief excerpts in connection with reviews or scholarly analysis or material supplied specifically for the purpose of being entered and executed on a computer system, for exclusive use by the purchaser of the work. Duplication of this publication or parts thereof is permitted only under the provisions of the Copyright Law of the Publisher's location, in its current version, and permission for use must always be obtained from Springer. Permissions for use may be obtained through RightsLink at the Copyright Clearance Center. Violations are liable to prosecution under the respective Copyright Law. The use of general descriptive names, registered names, trademarks, service marks, etc. in this publication does not imply, even in the absence of a specific statement, that such names are exempt from the relevant protective laws and regulations and therefore free for general use.

While the advice and information in this book are believed to be true and accurate at the date of publication, neither the authors nor the editors nor the publisher can accept any legal responsibility for any errors or omissions that may be made. The publisher makes no warranty, express or implied, with respect to the material contained herein.

Printed on acid-free paper

Springer is part of Springer Science+Business Media (www.springer.com)

Preface

The MUSME 2014, IFToMM-FelbIM–International Symposium on Multibody Systems and Mechatronics is the fifth event of a series that was started in 2002 as a conference activity mainly for promoting these topics in South American community. The first event was held at Universidad Panamericana de la Ciudad de México, Mexico in May 2002, the second was held at Federal University of Uberlandia, Brazil in March 2005, the third was hosted at Universidad Nacional de San Juan, Argentina, in April 2008, and the fourth was celebrated at Universidad Politecnica deValencia, Spain, in October 2011. This year the MUSME event has come to SUNEEO (Sistema de Universidades Estatales de Oaxaca) at UMAP Campus Huatulco, Oaxaca, under the auspices of Instituto Politecnico Nacional (IPN) and Universidad Autonoma de Queretaro, Mexico.

The MUSME aim was decided at the funding meeting in 2002 as: a conference stimulating integration between Mechatronics and Multibody Systems Dynamics disciplines; a forum for facilitating contacts among research people and students; and a match conference for communities from IFToMM (International Federation for the Promotion of Mechanism and Machine Science) and FelbIM (Federación Iberoamericana de Ingeniería Mecánica). In addition, since the beginning it has been considered preferable to have the MUSME Symposium in a location within South America, but without neglecting the possibility to bring MUSME in other parts of the world, since it is supported both by IFToMM and FelbIM.

The aim of the MUSME Symposium is to bring together researchers, industry professionals, and students from a broad ranges of disciplines referring to Mechatronics and Multibody Systems, in an intimate, collegial, and stimulating environment. Again, in the 2014 MUSME event we received a significant attention to the initiative, as can be seen by the fact that this Proceedings volume contains contributions by authors from all over the world.

The Proceedings volume of the MUSME Symposium is published within the Springer series on MMS (Mechanism and Machine Science) and contains 53 papers that have been selected from 63 submitted papers after peer review for oral

presentation. The accepted papers cover several aspects of the wide field of Multibody Systems and Mechatronics. Special attention has been given to organizing student sessions with good works from young researchers, who are still in the formation process.

This is the first time that the Proceedings is published by Springer whereas the previous proceedings were published as CD proceedings that nevertheless are available at the hosting institutions.

We would like to express grateful thanks to the members of the International Scientific Committee for MUSME Symposium for cooperating enthusiastically for the success of the MUSME 2014 event:

Prof. Marco Ceccarelli (Chair), Italy
Prof. Mario Acevedo, Mexico
Prof. Jorge A.C. Ambrósio, Portugal
Prof. Alberto Cardona, Argentina
Prof. Osvaldo H. Penisi, Argentina
Prof. João Carlos M. Carvalho, Brazil
Prof. Javier Cuadrado, Spain
Mario Fernandez Fernandez, Chile
Prof. Manfred Husty, Austria
Prof. Tatu Leinonen, Finland
Prof. Vicente Mata, Spain
Prof. Carlos Munares, Perú
Prof. Pietro Fanghella, Italy

We thank the authors who have contributed with interesting papers in several subjects, covering many fields of Multibody Systems and Mechatronics and, additionally, for their cooperation in revising papers in a short time in agreement with the reviewers' comments. We are grateful to the reviewers for the time and effort they spent in evaluating the papers with a very tight schedule that has permitted the publication of this Proceedings volume in time for the symposium event.

We thank Rector Modesto Seara Vazquez for accepting to host the MUSME 2014 event at SUNEI. We thank our colleagues for their help at the LARM Laboratory of Robotics and Mechatronics of University of Cassino and at the ESIME Ticoman del Instituto Politecnico Nacional. We thank the Director of ESIME Ticoman, Javier Roch Soto. We thank COFAA-IPN for its economic support for some activities of the MUSME event.

We also thank the auspices of IFToMM (International Federation for the Promotion of Mechanism and Machine Science) and FeIbIM (Federación Iberoamericana de Ingeniería Mecánica).

We thank the publisher and Editorial staff of Springer for accepting and helping the publication of this Proceedings volume, since the early step in 2012.

We are grateful to our families since without their patience and comprehension it would not have been possible for us to organize MUSME 2014, IFToMM-FeI-bIM–International Symposium on Multibody Systems and Mechatronics and this Proceedings volume.

June 2014

Marco Ceccarelli
Eusebio Eduardo Hernandez Martinez

Contents

Kinematic and Workspace-Based Synthesis of a 2-DOF Mechanism for Haptic Applications	1
R. Roberts and E. Rodriguez-Leal	
Fuzzy Logic Control on FPGA for Solar Tracking System	11
Ricardo Antonio-Mendez, Jesus de la Cruz-Alejo and Ollin Peñaloza-Mejia	
Dynamic Balancing of a Nutating Planetary Bevel Gear Train.	23
P. Fanghella, L. Bruzzone and S. Ellero	
Output Stabilization of Linear Systems with Disturbances.	35
Francisco Javier Bejarano and Jorge Dávila	
Development of a Heliostat for a Solar Tower Power Plant	45
Jorge A. García Pitol, Alicia Hernandez Gutierrez, Manuel Toledano Ayala, Juan C.A. Jáuregui Correa, Enma V. Godoy Avendaño and Oswaldo Mendoza Herbert	
Mechatronic Sizing of Ball-Screw Feed Drives	55
R. Hecker, D. Vicente and G. Flores	
Behavior of the Robot with Vibratory Excitation	67
T. Majewski and D. Szwedowicz	
Attitude Determination System Based on Vector Observations for Satellites Experiencing Sun-Eclipse Phases	75
J. Rodrigo Cordova-Alarcon, Mario A. Mendoza-Barcenas and Arturo Solis-Santome	

Nonlinear Identification of Inverted Pendulum System Using Volterra Polynomials	87
G. Ronquillo, G.J. Ríos Moreno, E. Hernández Martínez and M. Trejo Perea	
Multi-robot Exploration and Mapping Strategy in Underground Mines by Behavior Control	101
Antoni Mauricio, Ayrton Nieves, Yomar Castillo, Kenji Hilaraca, Christian Fonseca, Jhair Gallardo, Ricardo Rodríguez and Glen Rodríguez	
Modeling Online via Clustering and Fuzzy SVM.	111
J.C. Tovar, C.R. Mariaca and I. Álvarez Villalobos	
Cylindrical Contact Force Models for the Dynamics of Roller Chain Drives.	121
J. Ambrosio, C. Malça and A. Ramalho	
A Three-Dimensional Multibody Model of a Full Suspension Mountain Bike	133
B. Corves, J. Breuer, F. Schoeler and P. Inenlath	
Gear Shifting Strategies Co-simulations to Optimize Vehicle Performance and Fuel Consumption.	143
Jony J. Eckert, Fernanda C. Corrêa, Fabio M. Santiciolli, Eduardo S. Costa, Heron J. Dionísio and Franco G. Dedini	
Vibration Analysis of an Offshore Platform-Like Structure Excited by Earthquake	153
J. Enríquez-Zárate and G. Silva-Navarro	
Dynamic Parameter Identification in the Front Suspension of a Vehicle: On the Influence of Different Base Parameter Sets	165
L.A. Mejía, V. Mata, F. Valero, J. Ros and X. Iriarte	
An Alternative Method for the Optimum Dynamic Balancing of the Four-Bar Mechanism	177
Mario Acevedo, Eduardo Haro and Félix Martínez	
Behavior of Some Objects in Series with Dynamic Eliminators of Vibrations	189
Tadeusz Majewski	

Modeling, Analysis and Simulation of 3D Elastohydrodynamic Revolute Joints in Multibody Systems. 199
 P. Flores

Analysis of Experimental Data from Complex Multibody System 211
 J.C. Jáuregui-Correa, C.S. López Cajún and Mihir Sen

Reduced Energy Consumption in Induction Motors with Possible Mechatronic Applications 219
 G. Calzada-Lara and J. Álvarez-Gallegos

Modeling and Control of a Pendubot with Static Friction 229
 Sergio Sánchez-Mazuca, Israel Soto and Ricardo Campa

Design of Electronic Control Board to Obtain the Photovoltaic Module Power Voltage Curve as Temperature Function 241
 J. Vega-Pérez, S. Vega-Pérez and L. Castañeda-Aviña

A Robust Control Scheme Against Some Parametric Uncertainties for the NXT Ballbot 249
 R.A. García-García and M. Arias-Montiel

Fuzzy Logic Control on FPGA Using LabVIEW. 261
 Juan Carlos García-Montalva, Jesús de la Cruz-Alejo and Jorge Díaz-Salgado

High-Order Sliding Modes Based Linearization: An Application to Roll Autopilot 273
 J. Davila, A. Monsivais and A. Mosqueda

Proposal of Automated Inspection Using Camera in Process of VIN Validation 285
 L.R.S. Souza, R.M.M. Oliveira and M.H. Stoppa

Concept Design Process for Robotic Devices: The Case of an Assistive Robot 295
 H.A. Moreno Avalos, I.G. Carrera Calderón, S. Romero Hernández and V. Cruz Morales

Design and Construction of a Submarine with Five Degrees of Freedom 305
 Ortiz R. Floriberto, Barroeta Z. Carlos and J. Francisco Novoa C

Concurrent Structure-Control Design of Parallel Robots Using an Estimation of Distribution Algorithm	315
E. Chávez-Conde, S. Ivvan Valdez and Eusebio Hernández	
Emulation of Mechanical Structures Through a Multi-agent Robot System: An Overview	327
J. González-Sierra and E. Aranda-Bricaire	
Design and Construction of a Nouvelle Vertical Axis Wind Turbine Experimental Platform	339
Lourdes García, David Lara, Azahel Treviño, Gerardo Romero, José G. Rivera and Esmeralda Lopez	
Motion Analysis of a Six-Legged Robot Using the Bennett's Linkage as Leg	349
J.C.M. Carvalho and T.R. Silvestre	
Implementation of Force and Position Controllers for a 3DOF Parallel Manipulator	359
J. Cazalilla, M. Vallés, A. Valera, V. Mata and M. Díaz-Rodríguez	
Mechanical Reproduction of the Horse Movement from a Hippotherapy Cycle	371
C.S. López-Cajún, J.C. Jáuregui-Correa, C.A. González-Cruz and M. Rodríguez	
Identification of a Cylindrical Robot Using Recurrent Neural Networks	381
Carlos Román Mariaca Gaspar, Juan Eduardo Velázquez-Velázquez and Julio César Tovar Rodríguez	
New Design of Petal Type Deployable Space Mirror	391
V.I. Bujakas	
Corradino D'Ascanio and His Design of Vespa Scooter	399
M. Ceccarelli and G. Teoli	
Rigid Body Hyper-jerk Analysis Using Screw Theory	411
Jaime Gallardo-Alvarado and Mario A. Garcia-Murillo	
Joint Trajectory Optimization Using All Solutions of Inverse Kinematics of General 6-R Robots	423
U. Kuenzer and M.L. Husty	

Mill Setup Manual Aided by Augmented Reality 433
 F. Suárez-Warden, E. González Mendivil, H. Ramírez,
 L.E. Garza Nájera and G. Pantoja

Dimensional Synthesis of a Planar Parallel Manipulator Applied to Upper Limb Rehabilitation 443
 Ileana P. Corona-Acosta and Eduardo Castillo-Castaneda

Workspace Analysis of a Delta-Like Robot Using an Alternative Approach 453
 A. Gutiérrez-Preciado, M.A. González-Palacios
 and L.A. Aguilera-Cortés

Adaptive Low Cost Gravity Balanced Orthosis 465
 Giuseppe Cannella, Dina S. Laila and Christopher T. Freeman

Design and FEM Analysis of a Novel Humanoid Torso 477
 Daniele Cafolla and Marco Ceccarelli

Nonlinear Full-Car Model for Optimal Dynamic Design of an Automotive Damper 489
 Carlos A. Duchanoy, Carlos A. Cruz-Villar
 and Marco A. Moreno-Armendáriz

Design of a Parallel Mechanism for Knee Rehabilitation 501
 B.D. Chaparro-Rico, E. Castillo-Castaneda
 and R. Maldonado-Echegoyen

Design and Construction of a Translational Parallel Robot for Drilling Tasks 511
 R. Maldonado-Echegoyen and E. Castillo-Castaneda

A Solution to the Approximate Spherical Burmester Problem 521
 Jérémie Léger and Jorge Angeles

Mechatronic Design of a Mobile Robot and Non-Linear Control 531
 J. Hernández, J. Torres and S. Salazar

Decentralized Supervisory Control of an AMS Based on the ISA Standards 543
 E.G. Hernandez-Martinez, S.A. Foyo-Valdes, E.S. Puga-Velazquez
 and J.A. Meda-Campaña

A Planar Cobot Modelled as a Differential Algebraic System. 555
Omar Mendoza-Trejo and Carlos Alberto Cruz-Villar

**Design and Implementation of an Affective Computing
for Recognition and Generation of Behaviors in a Robot.** 567
Rodolfo Romero Herrera, Francisco Gallegos Funes
and Maria Adela Soto Alvarez del Castillo

Author Index 579

Kinematic and Workspace-Based Synthesis of a 2-DOF Mechanism for Haptic Applications

R. Roberts and E. Rodriguez-Leal

Abstract This paper presents the development of a mechanism aimed to haptic applications. The basic design proposed in this work is intended to interact with a finger without the use of a fixture attached to the body. This work investigates the theoretical workspace of a human index finger and proposes a two degree-of-freedom 7-bar linkage mechanism that is synthesized based on such workspace. The paper determines the closed-form solutions to the forward and inverse position, and presents a prototype that is built and tested as a proof of concept of the novel device. The workspace of the constructed mechanism is compared with theoretical models in order to assess their similarity and the viability of accelerometers as position sensing instruments is also tested.

Keywords Haptics · Workspace analysis · Kinematics · Human–machine interaction · Prototype

1 Introduction

The enhancement of the user-experience in virtual environments has been a highly studied topic in recent years [1, 2]. Audiovisual devices are capable to provide engaging interactive experiences to users, and can be classified as one-way or two-way communication systems, e.g. watching TV or playing videogames respectively. One of the most challenging issues in two-way communications is the saturation of the communication channels that result in the loss of information. To overcome this issue, a haptic device could be used as an alternative communication channel. For several decades, haptic devices have been commercially available for

R. Roberts (✉) · E. Rodriguez-Leal
Tecnológico de Monterrey, Monterrey, Mexico
e-mail: re.roberts.phd.mty@itesm.mx

E. Rodriguez-Leal
e-mail: ernesto.rodriguez@itesm.mx

different applications, e.g. using vibrotactile actuators in cell phones and pagers [3], or guiding tools that are designed to help soldiers to navigate in battlefields [4]. Moreover, the gaming industry is a niche for haptic devices, enhancing the multimedia experiences of players and providing a new sense of realism [5]. Furthermore, force feedback haptic devices have received a special interest from the medical community including applications such as palpation, needle insertion, laparoscopy, endoscopy, endovascular procedures or arthroscopy [6].

Several of the commercial single-point force feedback devices are designed to be manipulated using an entire hand, displaying three translational degrees-of-freedom (DOF), and can be provided with three additional rotational DOF [6, 7]. Some of the benefits of this type of devices include a workspace in which comfortable movement is allowed, and a mechanism design that is low weight while is capable to provide reliable force feedback. Some of the drawbacks that are encountered in single-point force feedback devices include accuracy limitations in multiple-object simulation, which is essential for object recognition in haptics [8, 9].

This paper describes the development and synthesis of the novel haptic device and is organized as follows: Sect. 2 presents a description of the desired characteristics and features of this mechanism. Section 3 performs a thorough mathematical analysis of the mechanism. A practical approach for conducting the synthesis of the mechanism is discussed in Sect. 4, where the workspace of a human finger is used to determine the dimensional parameters of the mechanism. Section 5 discusses the prototype and validates the theoretical workspace with experimental data. Finally, the paper presents conclusions and suggestions for further work.

2 Mechanism Description

The new haptic mechanism proposed in this paper considers the following features: (i) compact size suitable for finger movement, (ii) non-collapsibility, (iii) low mechanical impedance. A compact apparatus is desirable since a long term goal of this project is to build a multi-point haptic device. Hence, it is important to reproduce this mechanism five times within the workspace of a hand. A non-collapsible mechanism eliminates the inclusion of components that force contact with the finger. This feature is required in cases in which movement flexibility is desired. Finally, reducing inertia and friction in the device is desired to achieve a realistic haptic experience.

Figure 1a shows the proposed seven-link and six-joint mechanism, which can be thought as two four-bar mechanisms that share a common bar. The base is connected to link 2 with links 1 and 3 with the use of joints, while the platform is connected to link 2, with links 4 and 5. Note that all the axes of the joints are parallel to each other and to the Z axis. Consider that links 1, 3, 4 and 5 have a length l while link 2, the base and the platform have a length that is equal for the three elements, although the particular value of this parameter is irrelevant as the following equations will show. The abovementioned dimensional considerations

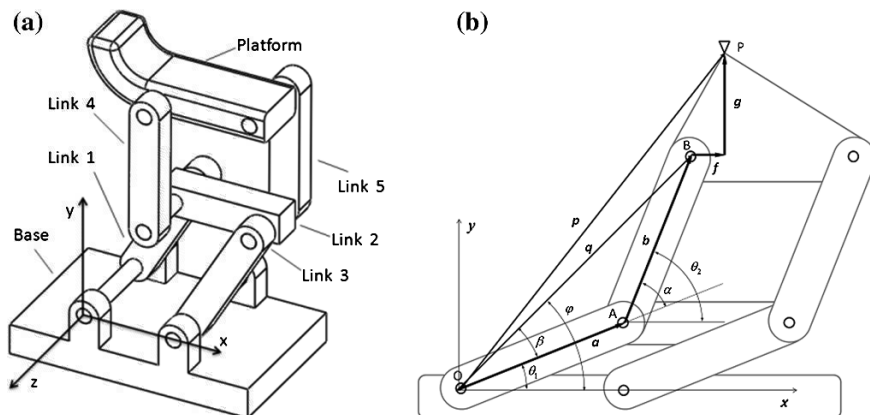


Fig. 1 a CAD model and b vector representation of the seven bar linkage

guarantee that the mechanisms comply with the Grashof condition [10]; they also assure that the base, platform, and link 2 remain parallel for all positions of the mechanism. Note that the joint connecting links 2 and 5 is active, meaning that a motor applies torque to this kinematic pair; this is also the case for the joint connecting the base and link 1. The following section includes the kinematics analysis that determines the closed-form solutions to the position, velocity and acceleration of the seven-bar mechanism.

3 Mechanism Kinematics

The forward *kinematics* consists in determining the position vector p of an arbitrary point P of the platform. See Fig. 1b for a vector representation of the mechanism. Note that for analysis convenience, all vectors lie on the XY plane and is possible to determine p as follows:

$$\mathbf{p} = [lc\theta_1 + lc\theta_2 + f, \quad ls\theta_1 + ls\theta_2 + g]^T \quad (1)$$

where f and g are the magnitudes of vectors f and g . θ_1 and θ_2 denote the angular position of the active joints connected to links 1, and 4, respectively. Note that links 1 and 3 are parallel, the same is true for links 4 and 5.

The *inverse kinematics* consists in finding the magnitude of the angular positions of the active joints for a given position of the platform. Consider from Fig. 1 that vector q describes the position of point B and can be expressed as:

$$\mathbf{q} = [lc\theta_1 + lc\theta_2, \quad ls\theta_1 + ls\theta_2]^T \quad (2)$$

where the magnitude q of vector q results in

$$q = |\mathbf{q}| = \sqrt{(lc\theta_1 + lc\theta_2)^2 + (ls\theta_1 + ls\theta_2)^2} = \sqrt{(l + lc\alpha)^2 + (ls\alpha)^2} \quad (3)$$

where α is the angular position of link 5, relative to link 1. Solving for α , φ , and β results in

$$\alpha = \text{acos}\left(\frac{q^2 - 2l^2}{2l^2}\right), \beta = \text{atan}\left(\frac{ls\alpha}{l + lc\alpha}\right), \text{ and } \varphi = \text{atan}\left(\frac{q_y}{q - f}\right) \quad (4)$$

where q_x and q_y are the X and Y components of q , respectively. The angular positions of the active joints θ_1 and θ_2 can be written as

$$\theta_1 = \varphi - \beta \quad \text{and} \quad \theta_2 = \alpha + \theta_1 \quad (5)$$

All the above calculations use vector q rather than p for simplicity. The mechanism design produces a constant translational relationship between these two vectors.

$$\mathbf{p} = [q_x + f \quad q_y + g]^T \quad (6)$$

Note that for any given point P the magnitudes f and g are constant and independent of θ_1 and θ_2 . The Jacobian matrix for the mechanism results in

$$\mathbf{J}_p = \mathbf{J}_q = \begin{bmatrix} -ls\theta_1 & -ls\theta_2 \\ lc\theta_1 & lc\theta_2 \end{bmatrix} \quad (7)$$

Note that the Jacobian of vectors p and q is identical. The study of singularities is fundamental for haptic mechanisms which are defined as the configurations where the matrices relating input and output parameters (Jacobian) become rank deficient [11]. Therefore is essential to identify all possible singularity configurations since they might lead to undesirable operation of the mechanism.

The singular configurations of the mechanism occur when the determinant $|\mathbf{J}|$ in Eq. (7) equals zero, resulting in

$$-l^2 s\theta_1 c\theta_2 + l^2 c\theta_1 s\theta_2 = 0 \quad (8)$$

By inspection of Eq. (8) is possible to determine that the singularity occurs when

$$\theta_1 = \theta_2 \quad (9)$$

$$\theta_1 = \theta_2 \pm \pi \quad (10)$$

Note that the first singularity configuration in Eq. (9) occurs when links 1 and 5 are aligned and the mechanism finds itself at the edge of its reachable workspace.

By using polar coordinates it is possible to observe the loss of one DOF of the mechanism in the singularity configuration. The second singularity conditions are met when link 1 has an angle of 180° relative to link 5. Note that the mechanism depicted in this work is unable to reach this condition due to mechanical constraints.

4 Mechanism Synthesis by Workspace Analysis

This section presents the synthesis of the mechanism following an approach based on the study of the human finger workspace in order to define the link dimension parameters for this mechanism. According to the literature, it is common to model a human finger as a three bar linkage with four rotational DOF where the first joint has two rotational DOF, the second and third joints have one DOF [12]. For the following workspace analysis, it is considered that each joint provides one DOF. The dimensional parameters of a human index finger and the range of angular displacement allowed by each of its joints differ unevenly among the human population [13]. However, the values used in this work represent a median and have been used in related work [12]. The mechanism selected to interact with the finger has to comply with various characteristics. The mechanism has to be safe; therefore the forces that the apparatus can exert cannot pass determined levels. The mechanism range has to intersect with the bulk of the finger workspace, although not completely. Low mass and friction are desired to optimize the haptic experience.

A configuration that complies with the mentioned characteristics is the seven bar mechanism described in the previous sections. Consider that the length and maximum angular displacement are optimized considering its interaction with the finger model. The synthesis of the seven bar mechanism is thus performed by iterating several combinations of dimensional parameters. The approach followed is to produce different mechanism workspaces and identify the best fit in the theoretical finger workspace. To show how the angle and length parameters modify the mechanism workspace, multiple combinations were studied. The lengths of links 1, 3, 4, and 5 are defined to be more than 30 mm; similarly the joints rotation range is required to be at least 150° . Given that the links have a width of 10 mm a simple cosine rule shows that for this angle, the base, link 2 and the platform have to be of at least 40 mm in length. This length is also applied to links 1, 3, 4 and 5 since it has been concluded that an acceptable length is between 30 mm and 50 mm. The mechanism with the mentioned dimensions is simulated using a Labview program to generate its theoretical workspace, which is compared with the model of the finger. The resulting intersection is presented in Fig. 2.

For the following analysis, the area of the mechanism and finger workspaces depicted in Fig. 2 are named m_A and f_A , respectively. The intersection between both workspaces referred as i_A . Note that f_A is exogenous and cannot be modified, and while the maximization of i_A is desired, conversely minimization of m_A is also preferred as it implies a more compact mechanism. To further explore this concept,

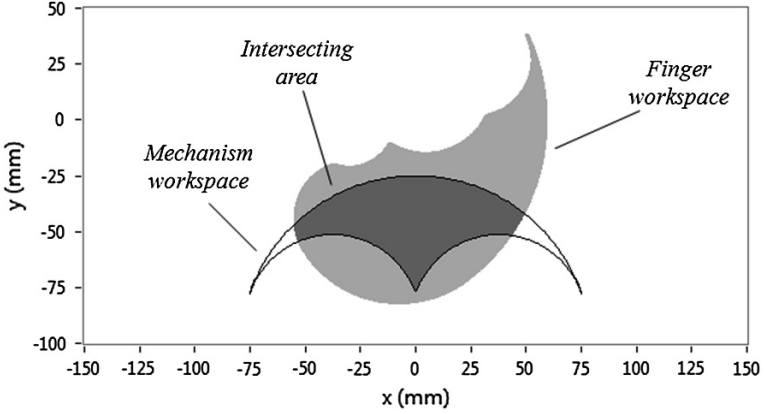


Fig. 2 Mechanism and finger workspaces and the intersecting area

two indexes are defined. The *finger utilization index* n_f is the ratio between the intersecting area i_A and the entire finger workspace f_A . Similarly, the *mechanism utilization index* n_m is the ratio between the intersecting area i_A and the entire mechanism workspace m_A . By definition both indexes can vary between 0 and 1 where the latter represents the complete use of the workspace.

$$n_f = \frac{i_A}{f_A} \quad \text{and} \quad n_m = \frac{i_A}{m_A} \quad (11)$$

In ordinary robotic applications the mechanism utilization is a parameter of interest; in haptic devices other parameters take importance such as finger utilization and device weight. These parameters are taken into account in the following equation:

$$\varepsilon = n_f + n_m - w_n \quad (12)$$

where ε is the proposed efficiency parameter and w_n is a normalized value of the apparatus mass. It is known that the device weight is proportional to the cube of the length l , given that proportions are kept. Due to the fact that n_f and n_m are non-linear, it is difficult to estimate them for complex workspaces as the ones considered in this document. Consequently, Fig. 3 presents the results of computational simulations that were performed in order to obtain n_f and ε_f for different values of l .

An inverse relation between n_f and n_m is observable in Fig. 3. Note that as l varies from 5 to 95 mm, n_f increases while n_m decreases; however, for any value of l equal or smaller than 25 mm, n_m saturates at 1, i.e. the finger workspace completely engulfs its mechanism counterpart. Extrapolation of the observed curves should yield a continuous decrease of n_m and an eventual saturation of n_f at 1; nevertheless for the purpose of this work, bar sizes above 100 mm are not suitable for a compact haptic device.

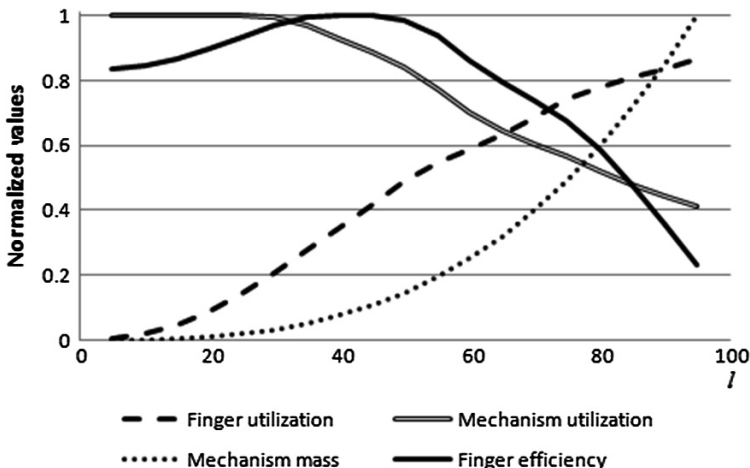


Fig. 3 Values of ϵ_f , n_m , and n_f for different mechanism dimension configurations

As the mechanism size increases, so does its mass. At low values this increase in weight is justified with a similar increase of finger utilization n_f ; above certain point however, this relationship breaks since the mass increases at a rate higher than the utilization. Considering this relationship, the abovementioned plot suggests an optimal value of 40 mm for the links of the haptic device.

This parameter is used in the construction of the haptic device, which is presented in the next section. Workspace analysis is validated comparing the theoretical model with real data.

5 Prototype

A prototype of the haptic device was constructed using the parameters defined in the previous sections. 3D printing technology was used in the construction of structural pieces, and DC motors are connected to the mechanism without the typical geared speed reduction. This produces a mechanism with low mechanical impedance, especially when the motors are inactive, which is essential in haptic simulations. Low mass helps to this effect as well as low friction joints. When active, the motors can apply a torque of up to 200 mNm, which is relatively high for this size of motors but commercially available nonetheless. The torque of the upper portion of the mechanism is transmitted with a toothed belt. The sprockets connected to the base and link 4 have a 2:1 ratio; which produces a torque increase of the same magnitude. The reactive force that the mechanism can apply to any user depends on the mechanism configuration and the torque applied to the motors. If the mechanism is in the singularity conditions described in Eqs. (9) and (10) and the user applies a force parallel to link 1, then the theoretical reactive force is infinite.

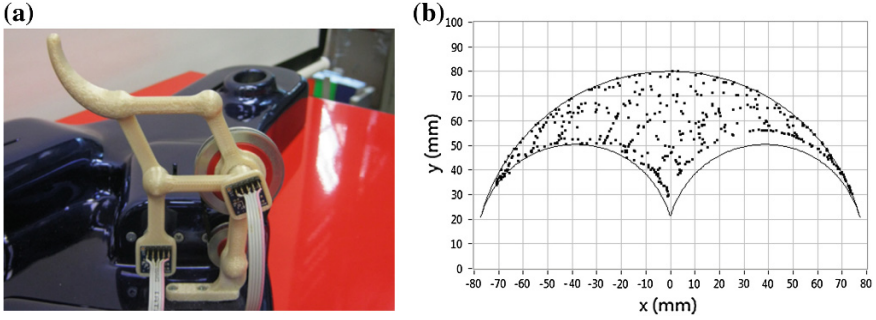


Fig. 4 a Prototype, and b comparison of the mechanism theoretical and experimental workspace

Conversely, the minimum reactive force occurs when the user applies force perpendicular to the links; in this case, the lower link will yield at 2.5 N. In case that the lower part of the mechanism is blocked (e.g. it has reached its angular limit), the upper mechanism will yield at 10 N due to the sprockets ratio and the shortening of the lever. The end-effector position is determined using Eq. (1). The values of l , f and g are constant for a given mechanism construction, while angles θ_1 and θ_2 are determined with accelerometers. The resolution of the position estimation depends on factors such as the accelerometer sensitivity and the characteristics of the analog to digital converter (ADC). Resolutions of less than 1° are possible using commercially available components such as a 10 bit ADC and a 300 mV/g accelerometer sensitivity. For the mechanism shown in Fig. 4a the accelerometers are placed on links 1 and 5.

The effectiveness of the accelerometer based positioning is tested by gathering their data as the end effector moves throughout its workspace. Five hundred points are estimated and compared with the theoretical workspace as shown in Fig. 4b. The overlap between the theoretical and experimental workspaces proves the effectiveness of the accelerometers as position measuring instruments. Note that the slight asymmetry can be attributed to the interference between link 5 and the platform. The latter has a diameter larger than the rest of the pieces in the joint that holds the sprocket. This feature reduces the angular liberty by a few degrees but does not affect the workspace shape.

6 Conclusions

This work presented the development of a seven-link mechanism force feedback device. The position analysis was performed and their equations obtained for solving the forward and inverse problems. Mechanism dimensions are suggested and tested using simulation software, performance indexes are proposed to compare various designs under an objective structure. An optimal configuration is obtained considering factors such as the device weight and the utilization of the finger and

the mechanism workspaces. The resulting parameters are used to construct the haptic device; the workspace of the resulting apparatus is compared with simulations and is shown that the CAD tools effectively predicted the emergent workspaces. Unlike conventional robots that use encoders to assess joint angles, the constructed apparatus uses accelerometers which effectively track the end effector position.

Acknowledgments The authors acknowledge the support received from Consejo Nacional de Ciencia y Tecnología (CONACyT), the e-Robots Research Chair from Tecnológico de Monterrey, and the Laboratorio de Robótica del Área Noreste y Centro de México.

References

1. Coles T, Meglan D, John N (2012) Adaptive virtual environments for neuropsychological assessment in serious games. *IEEE Trans Consum Electron* 58(2):197–204
2. Jones JA, Swan JE, Bolas M (2013) Peripheral stimulation and its effect on perceived spatial scale in virtual environments. *IEEE Trans Vis Comput Graph* 19(4):701–710
3. Levesque V, MacLean K (2011) Do-it-yourself haptics a practical introduction to haptics for consumer electronics. In: *International conference on consumer electronics*
4. Elliott L, van Erp J, Redden E, Duistermaat M (2010) Field-based validation of a tactile navigation device. *IEEE Trans Haptics* 3(2):78–87
5. Ramsamy P, Haffegge A, Jamieson R, Alexandrov V (2006) Using haptics to improve immersion in virtual environments. In: *Lecture notes in computer science*, vol 3992. Springer, Berlin, pp 603–609
6. Coles T, Meglan D, John N (2011) The role of haptics in medical training simulators: a survey of the state of the art. *IEEE Trans Haptics* 4(1):51–66
7. Nakao M, Kitamura R, Minato K (2010) A model for sharing haptic interaction. *IEEE Trans Haptics* 3(4):155–165
8. Plaisier M, Bergmann W, Kappers A (2010) Haptic object individuation. *IEEE Trans Haptics* 3(4):257–265
9. Pauluk D, Kitada R, Abramowicz A, Hamilton C, Lederman S (2011) Figure ground segmentation via haptic glance attributing initial finger contacts to objects or their supporting surfaces. *IEEE Trans Haptics* 4(1):2–13
10. Chang W, Lin C, Wu L (2005) A note on Grashof's theorem. *J Mar Sci Technol* 13(4):239–248
11. Gosselin C, Angeles J (1990) Singularity analysis of closed-loop kinematic chains. *IEEE Trans Robot Autom* 6(3):281–290
12. Abdel-Malek K, Yang K, Brand R, Tanbour E (2004) Towards understanding the workspace of human limbs. *Ergonomics* 47(13):1386–1405
13. Imrhan S, Sarder M, Mandahawi N (2009) Hand anthropometry in Bangladeshis living in America and comparisons with other populations. *Ergonomics* 52(8):987–998

Fuzzy Logic Control on FPGA for Solar Tracking System

Ricardo Antonio-Mendez, Jesus de la Cruz-Alejo
and Ollin Peñaloza-Mejia

Abstract This paper proposes a control technique for solar tracking system through the processing of fuzzy logic implemented on FPGA. The control is designed by calculating and storing membership values in lookup tables as integer values which are addressed in all stages involved in the fuzzy logic system according to Mamdani rules and max—min implication model. A defuzzification method using alpha-levels is proposed. Results are presented to validate the theoretical analysis.

Keywords Fuzzy logic · Alfa-levels · Sun tracking · FPGA · Mamdani

1 Introduction

Currently one of the mathematical disciplines with the highest number of followers is the fuzzy logic technique, which is the logic that uses expressions that are neither completely true nor completely false, i.e., is the logic applied to concepts that can take a any truth value in a set of values ranging between two extremes, absolute truth and complete falsity. Central to those based on the theory of fuzzy logic systems is that, unlike those based on classical logic, have the ability to acceptably reproduce the usual modes of reasoning, considering the certainty of a proposition is a matter of degree [1, 2]. Thus, the most attractive features of fuzzy logic are its

R. Antonio-Mendez (✉) · J. de la Cruz-Alejo · O. Peñaloza-Mejia
Mechatronic Department, Tecnológico de Estudios Superiores de Ecatepec,
Ecatepec, Estado de México, Mexico
e-mail: ric_xof@hotmail.com

J. de la Cruz-Alejo
e-mail: jesus_ch517@hotmail.com

O. Peñaloza-Mejia
e-mail: openaloza@tese.edu.mx

flexibility, tolerance for imprecision, its ability to model non-linear problems, and its basis in natural language.

In the other hand, implementation can be using general-purpose processors and depending fully on software in the realization of the system or adapting a general-purpose processor to perform dedicated fuzzy instructions. The approach is a trade-off between speed and generality. An alternative is using an exclusive hardware to perform the fuzzy operations as a closely related approach, through dedicated fuzzy circuits or Application Specific Integrated Circuits (ASICs). The approach leads to relatively high-speed operation, but is more costly. FPGAs are hardware devices used as user-programmable ASICs. The availability of software tools to generate efficient and flexible hardware description configurations automatically also brings easiness to the reconfiguration process. Moreover, FPGA designs can already be modeled, simulated and verified.

For the case of solar-concentrating collectors, some form of tracking mechanism is usually employed to enable the collector to follow the sun. This is done by monitoring the variation in degrees. Monitoring tracking systems can be classified based on their movement. This can be a single axis or two axes. In the case of a single-axis mode, the motion can be in various ways: east-west, north-south, or parallel to the earth's axis [2–4].

The paper describes the fastest way to program the FPGA based on the corresponding application program, which in this case is the code for the sun tracking control. Section 2 characteristics of the sensors and actuators, as well as communication protocols implemented on the FPGA program for each device are described. Section 3, experimental results are presented. Section 4, a comparison between defuzzification method used in the paper against centroid method is presented.

2 Fuzzy Logic System

Figures 1, 2 and 3 shows the block diagram of the overall system. Data acquisition is carried out by four brightness sensors which convert light intensity into digital output values. The output values are stored in internal registers which are accessed via the I²C communication protocol. It serves as interface for input values to the FLC. Outputs values of the FLC are the control actions which are communicated to the servomotors through the RS-232 protocol in digital mode, which contain the commands for positioning, according to the own configuration of each one servomotor. Hardware description, processing, setup and characteristics of the devices used in the system are presented next.

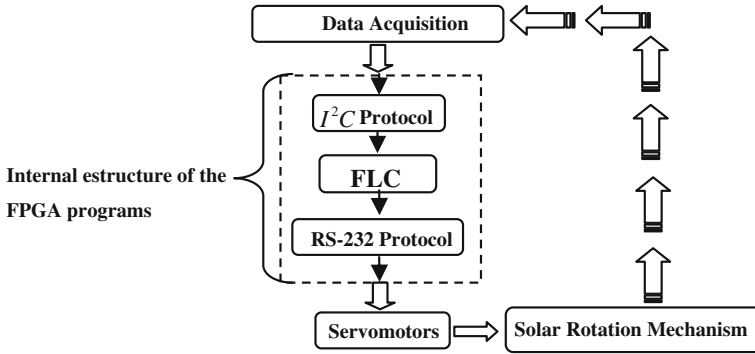


Fig. 1 Block diagram for the sun tracking system

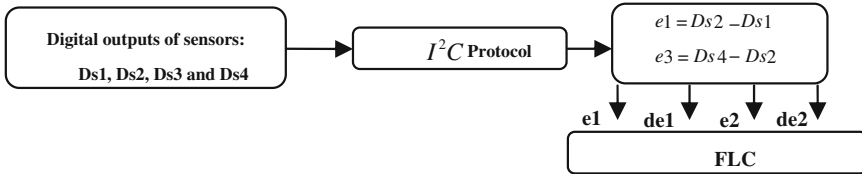


Fig. 2 Data acquisition for the FLC system

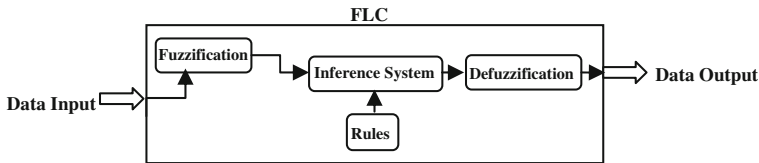


Fig. 3 Fuzzy logic control (FLC)

2.1 Fuzzification

The membership function chosen for this control was triangular, which is given by the parameters a, b, c as follows:

$$Triangulo(x; a, b, c) = \begin{cases} 0, & x \leq a \\ \frac{x-a}{b-a}, & a \leq x \leq b \\ \frac{c-x}{c-b}, & b \leq x \leq c \\ 0, & c \leq x \end{cases} \quad (1)$$

Using max—min operators, (1) can be represented as:

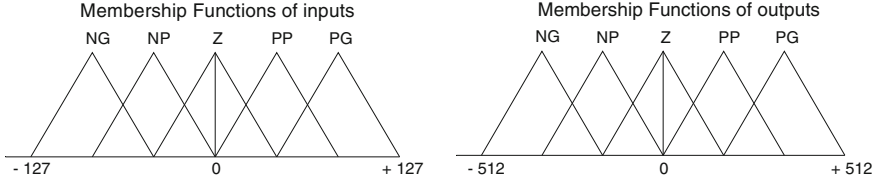


Fig. 4 Membership function for inputs and outputs

$$\text{triangulo}(x; a, b, c) = \max\left(\min\left(\frac{x-a}{b-a}, \frac{c-x}{c-b}\right), 0\right) \quad (2)$$

Using (2), the membership values for each input or output variable are obtained. For fuzzification stage, alpha-levels method was chosen. Input variables were expressed by five linguistic variables positive big (PB), positive small (PS), zero (ZO), negative small (NS) and negative big (NB). Membership functions of the fuzzy system are shown in Fig. 4. The universe of discussion for each input and output variable was expressed by five linguistic variables positive big (PB), positive small (PS), zero (ZO), negative small (NS) and negative big (NB).

The membership values are obtained through the programming of (2) in a spreadsheet on a pc. The resultant values are captured in look up tables which are stored in the internal program in order to be accessed to them in subsequent stages of the fuzzy logic system control. For example: Given an input value x , the membership value obtained is a floating-point value in a range between 0 and 1. This kind of value is complicated to implement in hardware, besides that involves the use of more resources on the device. So, the values are scaled depending on the resolution required, according to:

$$\left[\mu(x) = \text{Eq.}(2)_{\text{floating point}} \times 2^n - 1\right] = \mu(x)_{\text{integer value}} \quad (3)$$

This manner, using (3), floating point value is scaled to a $2^n - 1$ resolution, where n represent the number of bits used in the system. The code to obtain all membership values for negative_big set is as follows:

```

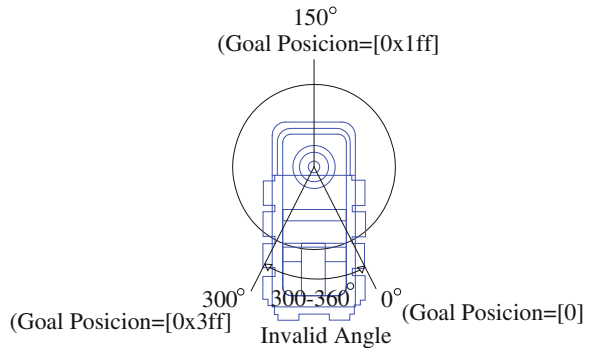
type Negative_Big is array (a to c) of integer range 0 to 2n - 1.
constant f_m1: Negative_Big := (a => 0, 1 => 6, 2 => 12, 4 => 18, ..., c => 2n - 1);
for i in a to c loop
  if (x = i) then
    μ(x) = f_m1(i)
  end if;
end loop;

```

where a and c are the parameters of the membership function given by (1) and (2).

In this case, because the sensors have a resolution of 8 bits ($2^8 - 1$), the input universe of discussion is partitioned from -127 to 127 as is shown in Fig. 4. A

Fig. 5 Range of movement of the servomotors



value of 0 indicates the lowest value of lighting and a value of 255 highest level. This indicates that the entry for the maximum value $e1 = Ds2 - Ds1$ either negative or positive is $2^n - 1$. Depending on whether $Ds2$ is greater than $Ds1$, the result is a positive number or otherwise $Ds1$ is greater than $Ds2$, which are negatives values. The universe from -512 to 512 indicated in Fig. 4 for the output of the system is proposed due to the movement of the servomotors have 1024 possible values. So, 1024 represents a position of 300° , 512 represents the midpoint, as shown in Fig. 5.

2.2 Rules

In this work, Mamdani’s method is used. In fuzzy logic controller a descriptive verbal rules (If–Then rules) are used to describe the relation among inputs and outputs, according to:

$$R^{(l)} : \text{IF } x_1 \text{ is } F_1^l \text{ and} \dots \text{and } x_n \text{ is } F_n^l \text{ THEN } y \text{ is } G^l \tag{4}$$

where:

- $(x_1 \dots x_n)$ Represent the input variable
- (y) Represent the output variable
- $(F \text{ y } G)$ Represent the membership function of fuzzy set.

So, rules are activated according to (4). Table 1 shows the corresponding rules for the fuzzy logic system.

Table 1 Corresponding rules for the fuzzy logic system

				<i>e1</i>		
		NG	NP	Z	PP	PG
	NG	NG	NP	NP	NP	NP
	NP	NP	Z	PP	NP	Z
<i>del</i>	Z	NP	PP	Z	PG	PP
	PP	Z	PP	PP	Z	PP
	PG	PP	PP	PP	PP	PG

2.3 Inference

The inference method chosen for this work is given by:

$$\mu_{A \rightarrow B}(x, y) = \min[\mu_A(x), \mu_B(y)] \quad (5)$$

It involves the comparison between two integer values, selecting the minimum value to activate rules. Now, in order to programming the fuzzy system, two arrays of rows and columns numbers which contain the maximum membership functions are programming. In these arrays are store the membership values which, corresponding to the fuzzy sets where they will be kept, i.e., if an input value falls within one or two fuzzy sets, the corresponding membership values for each one will be different in each set, therefore they will be stored in the array. Figure 6 shows the flow chart for the search and storing for all values in the array. The value *Data_inx* having *e1*, is stored in this variable and *a* and *c* values corresponding to the parameters of (1) (triangular membership function). These are the ranges in which the input value is looked *Data_inx*.

Whenever *Data_inx* has a constant value that matches the value previously stored in the tables corresponding to the membership function in question, this will be stored in the array *Wnx*. Table 2 shows vectors obtained from the search processes for *Data_inx* (*e1*) and *Data_iny* variable (*del*).

Taking into account the resulting vectors from the search, the inference process shown in Fig. 7, is performed. Inference process results are given in Table 3, as can be seen only the array of rules denominated $Wn_rules(i, j)$, are stored. This array has the same dimension as Table 1 have. This means that the input values which activate output linguistic rules are stored in the array $Wn_rules(i, j)$.

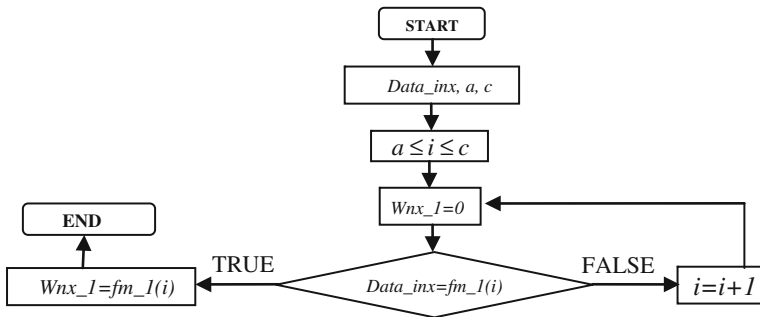


Fig. 6 Flow chart for the search process

Table 2 For data *inx* and data *iny*

Digital inputs	Vectors	<i>fm_1</i>	<i>fm_2</i>	<i>fm_3</i>	<i>fm_4</i>	<i>fm_5</i>
<i>Data_inx</i>	<i>Wnx=</i>	<i>Wnx_1</i>	<i>Wnx_2</i>	<i>Wnx_3</i>	<i>Wnx_4</i>	<i>Wnx_5</i>
<i>Data_iny</i>	<i>Wny=</i>	<i>Wny_1</i>	<i>Wny_2</i>	<i>Wny_3</i>	<i>Wny_4</i>	<i>Wny_5</i>

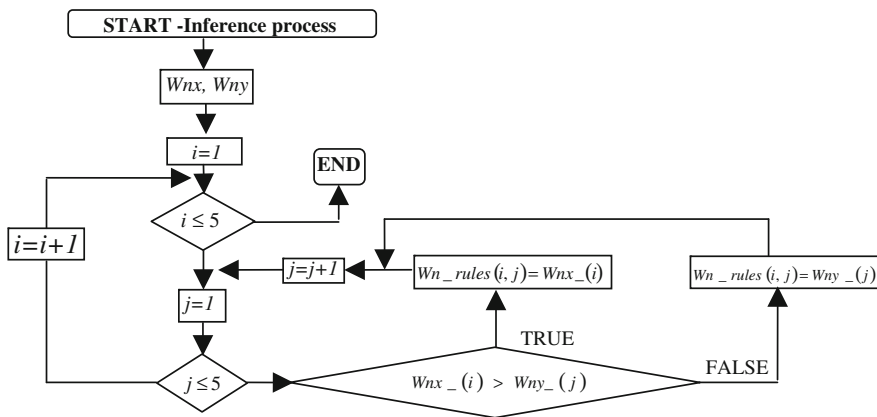


Fig. 7 Flow chart for the inference process

2.4 Aggregation

Aggregation stage is done by:

$$\mu_{B'}(y) = \max [\mu_{F_1'}(x_1), \dots, \mu_{F_n'}(x_n)] \tag{6}$$

It shows the global union of fuzzy sets and rules activated. It takes into account only those rules that have a non-zero value. The aggregation process is carried out by the method of maximum Eq. (6), for each one enabled rule whose value is